Crystal structure of pimecrolimus Form B, $C_{43}H_{68}ClNO_{11}$

Shivang Bhaskar,[1] Joseph T. Golab,[1] James A. Kaduk,[2,3,a)] Amy M. Gindhart,[4] and Thomas N. Blanton[4]
[1]*Illinois Mathematics and Science Academy, 1500 Sullivan Rd., Aurora, Illinois 60506-1000, USA*
[2]*Illinois Institute of Technology, 3101 S. Dearborn St., Chicago, Illinois 60616, USA*
[3]*North Central College, 131 S. Loomis St., Naperville, Illinois 60540, USA*
[4]*ICDD, 12 Campus Blvd., Newtown Square, Pennsylvania 19073-3273, USA*

(Received 24 October 2020; accepted 17 December 2020)

The crystal structure of pimecrolimus Form B has been solved and refined using synchrotron X-ray powder diffraction data and optimized using density functional techniques. Pimecrolimus crystallizes in the space group $P2_1$ (#4) with $a = 15.28864(7)$, $b = 13.31111(4)$, $c = 10.95529(5)$ Å, $\beta = 96.1542(3)°$, $V = 2216.649(9)$ Å^3, and $Z = 2$. Although there are an intramolecular six-ring hydrogen bond and some larger chain and ring patterns, the crystal structure is dominated by van der Waals interactions. There is a significant difference between the conformation of the Rietveld-refined and the DFT-optimized structures in one portion of the macrocyclic ring. Although weak, intermolecular interactions are apparently important in determining the solid-state conformation. The powder pattern is included in the Powder Diffraction File™ (PDF®) as entry 00-066-1619. This study provides the atomic coordinates to be added to the PDF entry.
[doi:10.1017/S088571562100004X]

Key words: pimecrolimus, Elidel, powder diffraction, Rietveld refinement, density functional theory

I. INTRODUCTION

Pimecrolimus (trade name Elidel) is used to treat atopic dermatitis (eczema) and other inflammatory skin diseases. It is usually prescribed in the form of a topical skin cream. Pimecrolimus binds to the receptor macrophilin-12 (FKBP-12) forming a complex that blocks the calcium-dependent signal transduction cascade mediated by calcineurin. Pimecrolimus weakens mast cell response, thus reducing inflammation on the region of skin where it is applied. Pimecrolimus is typically prescribed after a patient has not positively responded to other treatments. A small number of pimecrolimus users have reportedly developed skin cancer, but it is not known if this is the explicit result of pimecrolimus usage. More research is needed to determine whether long-term pimecrolimus administration increases the risk of any type of cancer. The IUPAC name (CAS Registry Number 137071-32-0) is (1*R*,9*S*,12*S*,13*R*,14*S*,17*R*,18*E*,21*S*,23*S*,24*R*,25*S*,27*R*)-12-[(*E*)-1-[(1*R*,3*R*,4*S*)-4-chloro-3-methoxycyclohexyl]prop-1-en-2-yl]-17-ethyl-1,14-dihydroxy-23,25-dimethoxy-13,19,21,27-tetramethyl-11,28-dioxa-4-azatricyclo[22.3.1.04,9]octacos-18-ene-2,3,10,16-tetrone. A two-dimensional molecular diagram is shown in Figure 1.

A star-quality powder pattern without atomic coordinates of pimecrolimus, based on a Le Bail fit to the synchrotron data of this study, is contained in the Powder Diffraction File (Gates-Rector and Blanton, 2019) as entry 00-066-1619. Pimecrolimus was reported in amorphous form in European Patent Application EP0427680A1 (Baumann, 1990; Sandoz). Amorphous pimecrolimus was also claimed in U.S. Patent 7,589,100B2 (Kovacsne-Mezei *et al.*, 2009; Teva), and a pattern of the amorphous phase was presented. Crystalline pimecrolimus was reported in U.S. Patent 6,423,722B2 (Dosenbach *et al.*, 2002; Novartis). Powder patterns for both Form A (a hydrate) and Form B (anhydrous) were provided.

This work was carried out as part of a project (Kaduk *et al.*, 2014) to determine the crystal structures of large-volume commercial pharmaceuticals and includes high-quality powder diffraction data for these pharmaceuticals in the Powder Diffraction File.

II. EXPERIMENTAL

Pimecrolimus was a commercial reagent, purchased from Carbosynth (Batch #FP270461501), and was used as-received. The white powder was packed into a 1.5-mm diameter Kapton capillary and rotated during the measurement at ~50 Hz. The powder pattern was measured at 295 K at beamline 11-BM (Lee *et al.*, 2008; Wang *et al.*, 2008) of the Advanced Photon Source at Argonne National Laboratory using a wavelength of 0.414157 Å from 0.5 to 50° 2θ with a step size of 0.001° and a counting time of 0.1 s step^{-1}.

The pattern was indexed on a monoclinic unit cell with $a = 15.329$, $b = 13.309$, $c = 10.952$ Å, $\beta = 96.2°$, $V = 2215.3$ Å^3, and $Z = 2$ using Jade 9.5 (MDI, 2014). Analysis of the systematic absences using EXPO2014 (Altomare *et al.*, 2013) suggested the space group $P2_1$. A reduced cell search in the Cambridge Structural Database (Groom *et al.*, 2016) yielded eight hits, but no pimecrolimus structures.

A pimecrolimus molecule was built using Spartan '18 (Wavefunction, 2018), saved as a .mol2 file, and converted

a)Author to whom correspondence should be addressed. Electronic mail: kaduk@polycrystallography.com

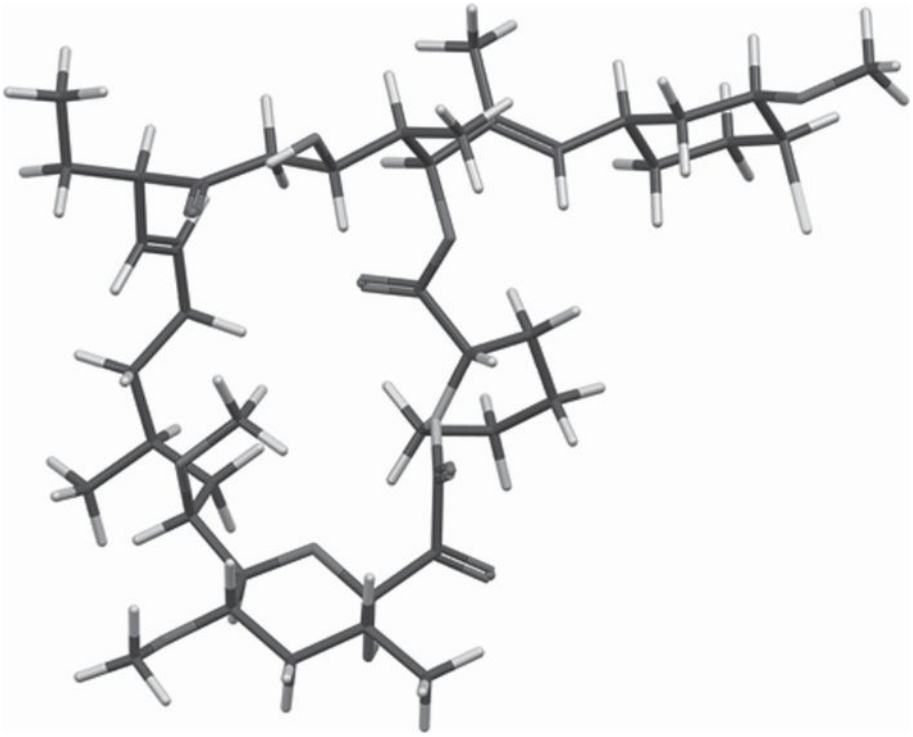

Figure 1. The molecular structure of pimecrolimus. Carbon is presented in dark green, hydrogen in white, nitrogen in blue, oxygen in red, and chloride in light green.

to .fh and .mop files using OpenBabel (O'Boyle *et al.*, 2011). Many attempts to solve the structure by Monte Carlo-simulated annealing techniques using several different programs yielded plausible, but ultimately unsatisfactory, structure models. The pimecrolimus molecule was downloaded as Structure2D_CID_6509979.sdf from PubChem. The 2D model was converted to 3D using Spartan, and the local minimum energy conformation was computed. The conformations of the two models (PubChem and manually built) were very different. Attempts to solve the structure using the 6509979 model also yielded plausible, but unsatisfactory (*wR* in the mid-teens) models. Close examination of the models used by FOX (Favre-Nicolin and Černý, 2002), DASH (David *et al.*, 2006), and EXPO2014-simulated annealing revealed an unexpectedly small number of torsional degrees of freedom. The C59–C60 bond in the large ring was broken, and the structure solutions attempted with more torsional degrees of freedom. In two of the 100 solutions from DASH, the ends of the broken ring were close together. The bond was manually remade using Materials Studio (Dassault Systèmes, 2018), and the structure was optimized using the Forcite module. Refinement was begun from this model.

Rietveld refinement was carried out using GSAS-II (Toby and Von Dreele, 2013). Only the 1.2–20.0° portion of the pattern was included in the refinement (d_{min} = 1.192 Å). The *y*-coordinate of C2 was fixed to define the origin. All non-H-bond distances and angles were subjected to restraints, based on a Mercury/Mogul Geometry Check (Bruno *et al.*, 2004; Sykes *et al.*, 2011) of the molecule. The results were exported to a .csv file. The Mogul average and standard deviation for each quantity were used as the restraint parameters, and were incorporated using the new feature Restraints/Edit Restraints/Add MOGUL Restraints, which reads the bond distance and angle restraints from the csv file. The restraints contributed 10.3% to the final χ^2. The hydrogen atoms were included in calculated positions, which were recalculated during the refinement using Materials Studio (Dassault Systèmes, 2018). The positions of the active hydrogen atoms were deduced by analysis of potential hydrogen bonding patterns. The U_{iso} of the non-H atoms were grouped by chemical similarity. The U_{iso} for each hydrogen atom was constrained to be 1.3× that of the heavy atom to which it is attached. The background was modeled using a four-term shifted Chebyshev polynomial, with two peaks at 1.42 (sharp) and 5.31° (broad) 2θ to model the scattering from the Kapton capillary.

The final refinement (begun from the result of the DFT calculation) of 196 variables using 18 802 observations and 143 restraints yielded the residuals *R*wp = 0.1192 and GOF = 1.68. The largest peak (0.19 Å from Cl16) and hole (1.48 Å from C60) in the difference Fourier map were 0.60 and −0.58(10) éÅ^{-3}. The Rietveld plot is included in Figure 2. The largest errors in the fit are in the positions of some of the low-angle peaks and probably represent the changes in the specimen during the measurement.

A density functional geometry optimization (fixed experimental unit cell) was carried out using VASP (Kresse and Furthmüller, 1996) through the MedeA graphical interface (Materials Design, 2016). The calculation was carried out on 16 2.4 GHz processors (each with 4 Gb RAM) of a 64-processor HP Proliant DL580 Generation 7 Linux cluster at North Central College. The calculation used the GGA-PBE functional, a plane wave cutoff energy of 400.0 eV, and a *k*-point spacing of 0.5 Å^{-1} leading to a 1 × 1 × 2 mesh, and took ∼81 h. A single-point density functional calculation on the VASP-optimized structure was carried out using CRYSTAL14 (Dovesi *et al.*, 2014). The basis sets for the H, C, N, and O atoms were those of Gatti *et al.* (1994), and the basis set for Cl was that of Peintinger *et al.* (2013).

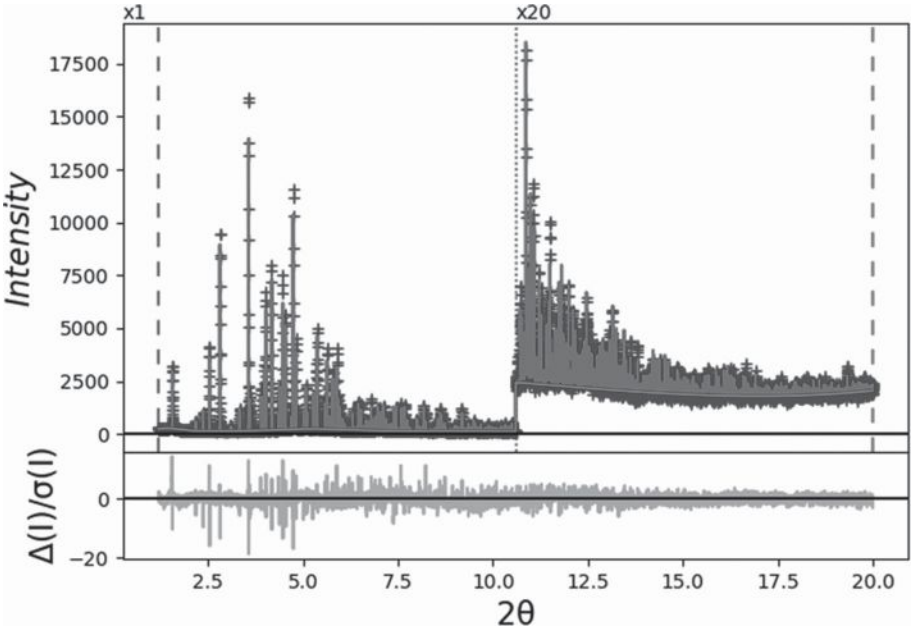

Figure 2. The Rietveld plot for the refinement of pimecrolimus. The blue crosses represent the observed data points, and the green line is the calculated pattern. The cyan curve is the normalized error plot. The vertical scale has been multiplied by a factor of 20× for 2θ >10.6°.

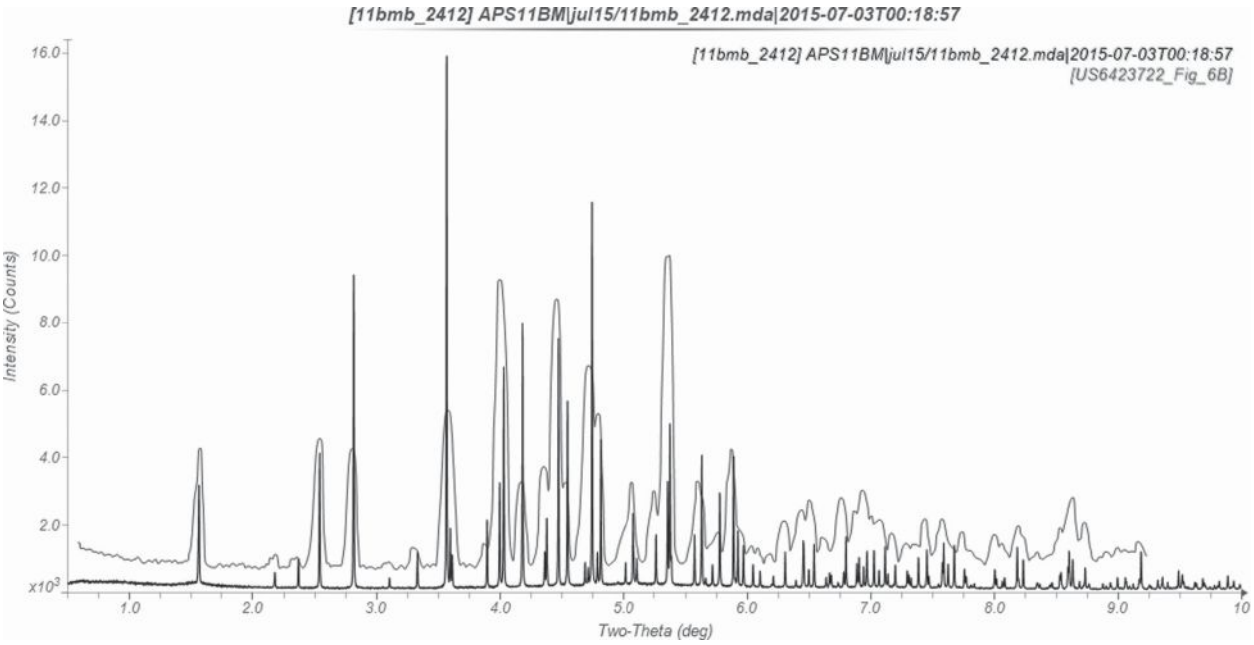

Figure 3. Comparison of the synchrotron pattern of pimecrolimus to the pattern of Form B reported by Dosenbach *et al.* (2002; Novartis). The published pattern was digitized using UN-SCAN-IT (Silk Scientific, 2013) and scaled to the synchrotron wavelength of 0.414157 Å using MDI JADE Pro (MDI, 2019).

The calculation was run on eight 2.1 GHz Xeon cores (each with 6 Gb RAM) of a 304-core Dell Linux cluster at IIT, using eight *k*-points and the B3LYP functional, and took ~34 h.

III. RESULTS AND DISCUSSION

This synchrotron powder pattern of pimecrolimus matches that reported for Form B by Dosenbach *et al.* (2002; Novartis) well enough to conclude that they correspond to the same material (Figure 3). The refined atom coordinates of pimecrolimus and the coordinates from the DFT optimization have been deposited with ICDD. The root-mean-square (rms) Cartesian displacement of the non-hydrogen atoms in the Rietveld-refined and DFT-optimized structures is 0.354 Å (Figure 4), and the maximum displacement is 1.076 Å, at C59. This difference represents a difference in conformation of this part of the macrocycle. The agreement between the refined and optimized structures is at the upper end of the expected range for correct structures (van de Streek and Neumann, 2014). This discussion concentrates on the CRYSTAL-optimized structure. The asymmetric unit (with

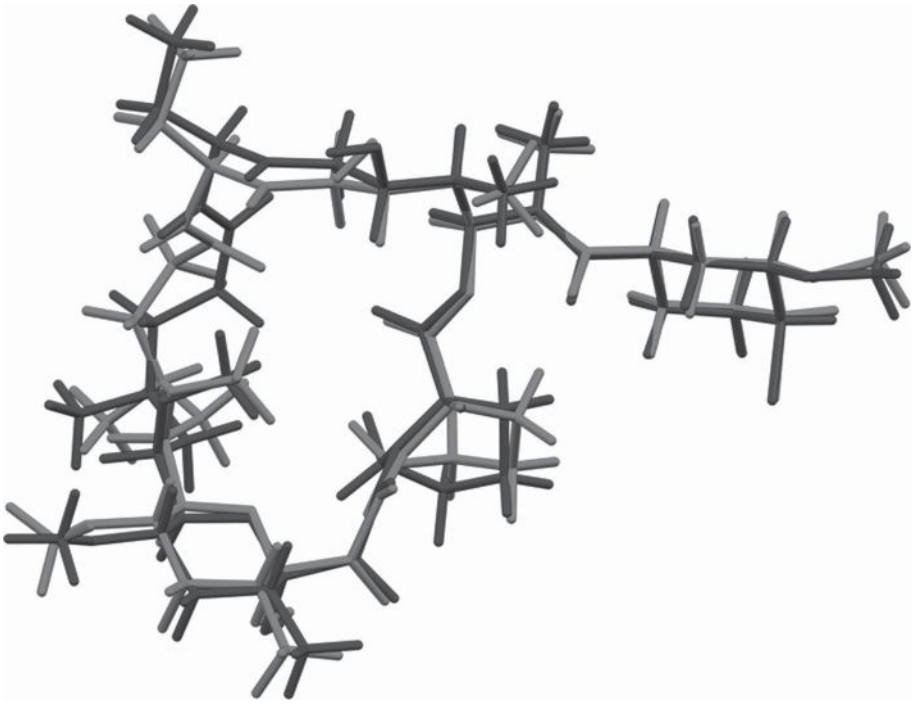

Figure 4. Comparison of the Rietveld-refined (red) and VASP-optimized (blue) structures of pimecrolimus. The rms Cartesian displacement is 0.354 Å.

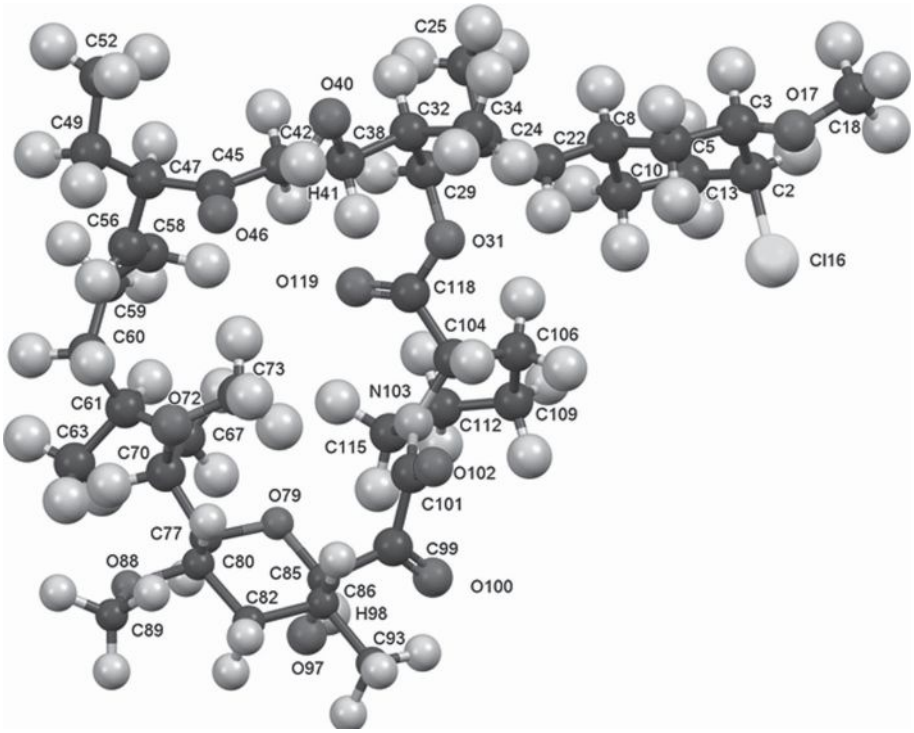

Figure 5. The asymmetric unit of pimecrolimus Form B, with the atom numbering. The atoms are represented by 50% probability spheroids.

atom numbering) is illustrated in Figure 5, and the crystal structure is presented in Figure 6.

The crystal of this large complex molecule is difficult to visualize in a static image (Figure 6). Although there are an intramolecular six-ring hydrogen bond and some larger chain and ring patterns, the structure is dominated by van der Waals interactions.

All of the bond distances and most of the bond angles and torsion angles in pimecrolimus fall within the normal ranges indicated by a Mercury Mogul Geometry check (Macrae *et al.*, 2008). The O31–C29–C32 angle of 109.5° [average = 106.9 (11)°; *Z*-score = 3.1] is flagged as unusual. This lies at the edge of a narrow distribution of similar angles. The C29–O31–C118–C104 torsion angle lies in the tail of a narrow

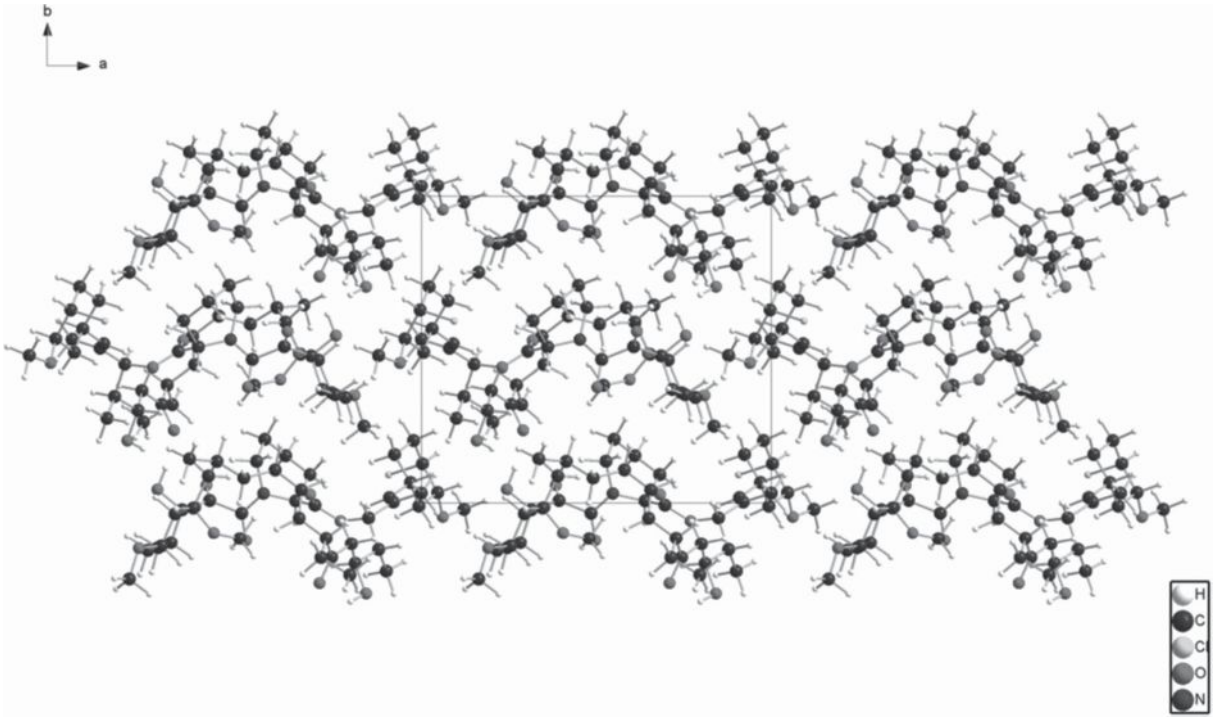

Figure 6. The crystal structure of pimecrolimus Form B, viewed down the *c*-axis.

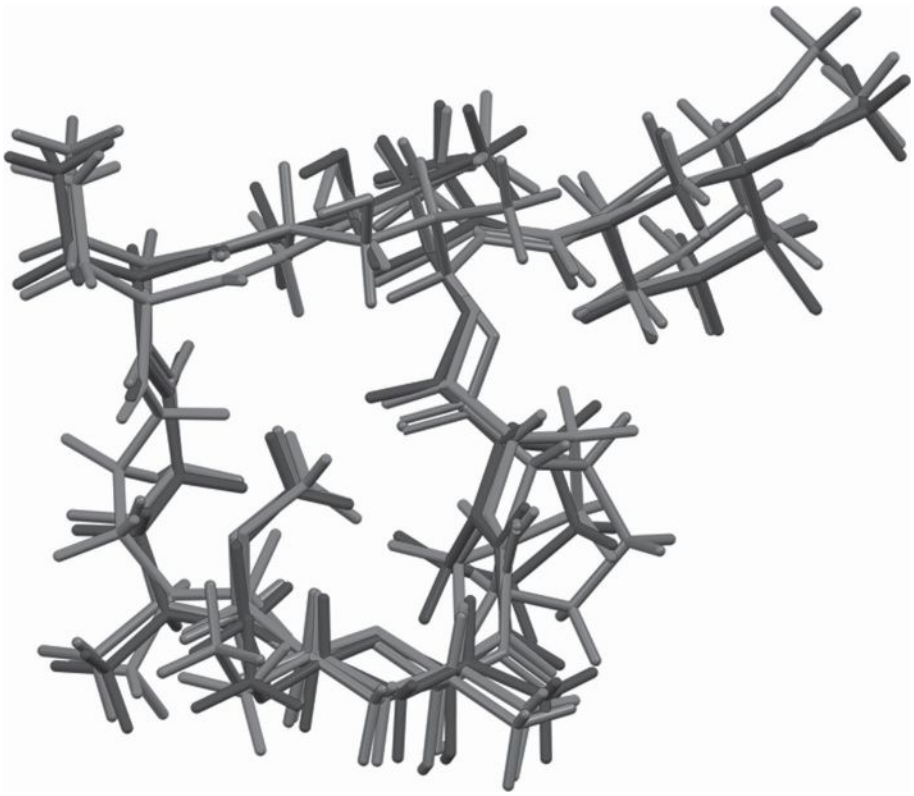

Figure 7. Comparison of the Rietveld-refined (red), DFT-optimized solid-state (blue), and DFT-optimized local minimum isolated molecule (green) structures of pimecrolimus.

planar distribution. The C58–C56–C47–C45 and C56–C58–C59–C60 torsion angles lie in the tails of broad distributions. The O100–C99–C85–C86, O79–C85–C99–C101, and C86–C85–C99–C101 torsion angles lie in the tails of distributions of only a few similar torsion angles. The O40–C38–C32–C29 and C42–C38–C32–C34 torsion angles are truly unusual.

Quantum chemical geometry optimization of the pimecrolimus molecule (DFT/B3LYP/6-31G*/water) using Spartan

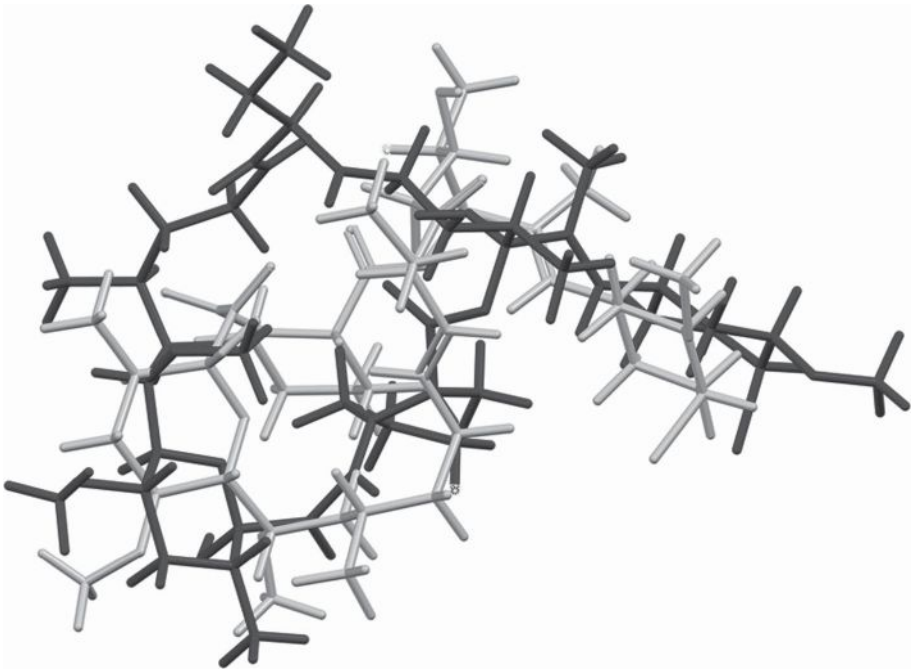

Figure 8. Comparison of the DFT-optimized solid-state structure of pimecrolimus (blue) and the global minimum energy conformation of an isolated molecule (orange).

'18 (Wavefunction, 2018) indicated that the observed solid-state conformation is 8.6 kcal mol^{-1} higher in energy than the local minimum. The local minimum is much more similar to the DFT-optimized structure at C59 than to the Rietveld-refined structure (Figure 7) but differs significantly in other places in the molecule. The minimum energy conformation of an isolated pimecrolimus molecule is very different than that observed in the solid state (Figure 8). The differences show that, although weak, the intermolecular interactions are important in determining the solid-state conformation.

Analysis of the contributions to the total crystal energy using the Forcite module of Materials Studio (Dassault Systèmes, 2018) suggests that bond, angle, and torsion distortion terms contribute to the intramolecular deformation energy, as might be expected in a macrocyclic fused-ring system. The intermolecular energy is dominated by van der Waals and electrostatic repulsions, which in this force-field-based analysis include hydrogen bonds. The hydrogen bonds are better analyzed using the results of the DFT calculation.

There are only two classical hydrogen bonds (Table I). The hydroxyl group O97–H98 acts as a donor in an intermolecular hydrogen bond to the ketone oxygen O46. The hydroxyl group O40–H41 acts a donor in an intramolecular hydrogen bond to the same ketone O46. The energies of these O–H···O hydrogen bonds were calculated from the Mulliken overlap populations using the correlation of Rammohan and Kaduk (2018).

The volume enclosed by the Hirshfeld surface (Figure 9; Hirshfeld, 1977; Turner *et al.*, 2017) is 1097.53 $Å^3$, 99.03% of half of the unit cell volume. The molecules are thus more loosely packed than usual. Most of the significant close contacts (red in Figure 9) involve the hydrogen bonds, and most intermolecular contacts are larger than the sums of van der Waals radii. The volume/non-hydrogen atom is rather large at 19.8 $Å^3$.

The Bravais–Friedel–Donnay–Harker (Bravais, 1866; Friedel, 1907; Donnay and Harker, 1937) morphology suggests that we might expect blocky morphology for pimecrolimus, with {100} as major faces. A fourth-order spherical harmonic model for preferred orientation was incorporated into the refinement. The texture index was 1.021, indicating that preferred orientation was slight in this rotated capillary specimen. The powder pattern of pimecrolimus from a Le Bail fit to this synchrotron data set is included in the Powder Diffraction File as entry 00-066-1619.

IV. DEPOSITED DATA

The Crystallographic Information Framework (CIF) files containing the results of the Rietveld refinement (including the raw data) and the DFT geometry optimization were deposited with the ICDD. The data can be requested at info@icdd.com.

TABLE I. Hydrogen bonds (CRYSTAL14) in pimecrolimus.

H-bond	D–H (Å)	H···A (Å)	D···A (Å)	D–H···A (°)	Overlap (é)	E (kcal mol^{-1})
O97–H98···O46	0.987	1.826	2.764	157.4	0.044	11.5
O40–H41···O46	0.981	1.982[a]	2.769	135.7	0.015	6.7

[a]Intramolecular.

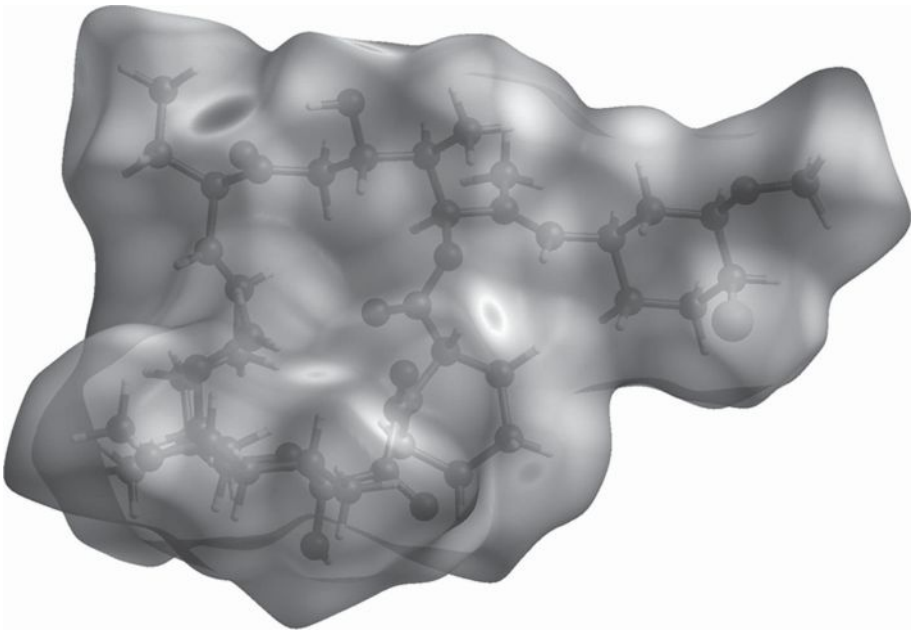

Figure 9. The Hirshfeld surface of pimecrolimus. Intermolecular contacts longer than the sums of the van der Waals radii are colored blue, and contacts shorter than the sums of the radii are colored red. Contacts equal to the sums of radii are white.

ACKNOWLEDGEMENTS

The use of the Advanced Photon Source at Argonne National Laboratory was supported by the U.S. Department of Energy, Office of Science, Office of Basic Energy Sciences under Contract No. DE-AC02-06CH11357. This work was partially supported by the International Centre for Diffraction Data. We thank Lynn Ribaud and Saul Lapidus for their assistance in the data collection and Andrey Rogachev for the use of computing resources at IIT.

CONFLICTS OF INTEREST

The authors have no conflicts of interest to declare.

Altomare, A., Cuocci, C., Giacovazzo, C., Moliterni, A., Rizzi, R., Corriero, N., and Falcicchio, A. (**2013**). "EXPO2013: a kit of tools for phasing crystal structures from powder data," J. Appl. Crystallogr. **46**, 1231–1235.

Baumann, K. (**1990**). "Heteroatoms-containing tricyclic compounds," European Patent Application EP0427680.

Bravais, A. (**1866**). *Etudes Cristallographiques* (Gauthier Villars, Paris).

Bruno, I. J., Cole, J. C., Kessler, M., Luo, J., Motherwell, W. D. S., Purkis, L. H., Smith, B. R., Taylor, R., Cooper, R. I., Harris, S. E., and Orpen, A. G. (**2004**). "Retrieval of crystallographically-derived molecular geometry information," J. Chem. Inf. Sci. **44**, 2133–2144.

Dassault Systèmes (**2018**). *Materials Studio 2019* (BIOVIA, San Diego, CA).

David, W. I. F., Shankland, K., van de Streek, J., Pidcock, E., Motherwell, W. D. S., and Cole, J. C. (**2006**). "DASH: a program for crystal structure determination from powder diffraction data," J. Appl. Crystallogr. **39**, 910–915.

Donnay, J. D. H. and Harker, D. (**1937**). "A new law of crystal morphology extending the law of Bravais," Am. Mineral. **22**, 446–447.

Dosenbach, C., Grassberger, M., Hartmann, O., Horvath, A., Mutz, J.-P., Penn, G., Pfeiffer, S., and Wieckhusen, D. (**2002**). "Crystalline macrolides and process for their preparation," U.S. Patent 6,423,722B1.

Dovesi, R., Orlando, R., Erba, A., Zicovich-Wilson, C. M., Civalleri, B., Casassa, S., Maschio, L., Ferrabone, M., De La Pierre, M., D-Arco, P., Noël, Y., Causà, M., and Kirtman, B. (**2014**). "CRYSTAL14: a program for the ab initio investigation of crystalline solids," Int. J. Quantum Chem. **114**, 1287–1317.

Favre-Nicolin, V. and Černý, R. (**2002**). "FOX, 'Free Objects for crystallography: a modular approach to ab initio structure determination from powder diffraction'," J. Appl. Crystallogr. **35**, 734–743.

Friedel, G. (**1907**). "Etudes sur la loi de Bravais," Bull. Soc. Fr. Mineral. **30**, 326–455.

Gates-Rector, S. and Blanton, T. (**2019**). "The powder diffraction file: a quality materials characterization database," Powd. Diffr. **39**(4), 352–360.

Gatti, C., Saunders, V. R., and Roetti, C. (**1994**). "Crystal-field effects on the topological properties of the electron-density in molecular crystals – the case of urea," J. Chem. Phys. **101**, 10686–10696.

Groom, C. R., Bruno, I. J., Lightfoot, M. P., and Ward, S. C. (**2016**). "The Cambridge Structural Database," Acta Crystallogr. Sect. B: Struct. Sci. Cryst. Eng. Mater. **72**, 171–179.

Hirshfeld, F. L. (**1977**). "Bonded-atom fragments for describing molecular charge densities," Theor. Chem. Acta **44**, 129–138.

Kaduk, J. A., Crowder, C. E., Zhong, K., Fawcett, T. G., and Suchomel, M. R. (**2014**). "Crystal structure of atomoxetine hydrochloride (Strattera), $C_{17}H_{22}NOCl$," Powd. Diffr. **29**(3), 269–273.

Kovacsne-Mezei, A., Racz, C. N., Aronhime, J., Gyollai, V., Molnar, S., and Pinchasov, M. (**2009**). "Non-hygroscopic and powdery amorphous pimecrolimus," U.S. Patent 7,589,100B2.

Kresse, G. and Furthmüller, J. (**1996**). "Efficiency of ab-initio total energy calculations for metals and semiconductors using a plane-wave basis set," Comput. Mater. Sci. **6**, 15–50.

Lee, P. L., Shu, D., Ramanathan, M., Preissner, C., Wang, J., Beno, M. A., Von Dreele, R. B., Ribaud, L., Kurtz, C., Antao, S. M., Jiao, X., and Toby, B. H. (**2008**). "A twelve-analyzer detector system for high-resolution powder diffraction," J. Synch. Radiat. **15**(5), 427–432.

Macrae, C. F., Bruno, I. J., Chisholm, J. A., Edington, P. R., McCabe, P., Pidcock, E., Rodriguez-Monge, L., Taylor, R., van de Streek, J., and Wood, P. A. (**2008**). "Mercury CSD 2.0 – new features for the visualization and investigation of crystal structures," J. Appl. Crystallogr. **41**, 466–470.

Materials Design (**2016**). *MedeA 2.20.4* (Materials Design Inc., Angel Fire, NM).

MDI (**2014**). *Jade 9.5* (Materials Data Inc., Livermore, CA).

MDI (**2019**). JADE *Pro Version 7.7 (Computer Software)* (Materials Data, Livermore, CA).

O'Boyle, N., Banck, M., James, C. A., Morley, C., Vandermeersch, T., and Hutchison, G. R. (**2011**). "Open babel: an open chemical toolbox," J. Chem. Informatics **3**, 33. doi:10.1186/1758-2946-3-33.

Peintinger, M. F., Vilela Oliveira, D., and Bredow, T. (**2013**). "Consistent Gaussian basis sets of triple-zeta valence with polarization quality for solid-state calculations," J. Comput. Chem. **34**, 451–459.

Rammohan, A. and Kaduk, J. A. (**2018**). "Crystal structures of alkali metal (Group 1) citrate salts," Acta Crystallogr. Sect. B: Crystallogr. Eng. Mater. **74**, 239–252. doi:10.1107/S2052520618002330.

Silk Scientific (**2013**). *UN-SCAN-IT 7.0* (Silk Scientific Corporation, Orem, UT).

Sykes, R. A., McCabe, P., Allen, F. H., Battle, G. M., Bruno, I. J., and Wood, P. A. (**2011**). "New software for statistical analysis of Cambridge Structural Database data," J. Appl. Crystallogr. **44**, 882–886.

Toby, B. H. and Von Dreele, R. B. (**2013**). "GSAS II: the genesis of a modern open source all purpose crystallography software package," J. Appl. Crystallogr. **46**, 544–549.

Turner, M. J., McKinnon, J. J., Wolff, S. K., Grimwood, D. J., Spackman, P. R., Jayatilaka, D., and Spackman, M. A. (**2017**). *CrystalExplorer17* (University of Western Australia). Available at: http://hirshfeldsurface.net.

van de Streek, J. and Neumann, M. A. (**2014**). "Validation of molecular crystal structures from powder diffraction data with dispersion-corrected density functional theory (DFT-D)," Acta Crystallogr. Sect. B: Struct. Sci. Crystallogr. Eng. Mater. **70**(6), 1020–1032.

Wang, J., Toby, B. H., Lee, P. L., Ribaud, L., Antao, S. M., Kurtz, C., Ramanathan, M., Von Dreele, R. B., and Beno, M. A. (**2008**). "A dedicated powder diffraction beamline at the advanced photon source: commissioning and early operational results," Rev. Sci. Instrum. **79**, 085105.

Wavefunction, Inc. (**2018**). Spartan '18 Version 1.2.0 (Wavefunction Inc., Irvine, CA).